

Soft Matter

Accepted Manuscript



This is an *Accepted Manuscript*, which has been through the Royal Society of Chemistry peer review process and has been accepted for publication.

Accepted Manuscripts are published online shortly after acceptance, before technical editing, formatting and proof reading. Using this free service, authors can make their results available to the community, in citable form, before we publish the edited article. We will replace this *Accepted Manuscript* with the edited and formatted *Advance Article* as soon as it is available.

You can find more information about *Accepted Manuscripts* in the [Information for Authors](#).

Please note that technical editing may introduce minor changes to the text and/or graphics, which may alter content. The journal's standard [Terms & Conditions](#) and the [Ethical guidelines](#) still apply. In no event shall the Royal Society of Chemistry be held responsible for any errors or omissions in this *Accepted Manuscript* or any consequences arising from the use of any information it contains.

Cooperative breakups induced by drop-to-drop interactions in one-dimensional flows of drops against micro-obstacles[†]

Alexandre Schmit,^a Louis Salkin,^a Laurent Courbin,^{a,‡} and Pascal Panizza^{a,§}

Received Xth XXXXXXXXXXXX 20XX, Accepted Xth XXXXXXXXXXXX 20XX

First published on the web Xth XXXXXXXXXXXX 200X

DOI: 10.1039/b000000x

Depending on the capillary number at play and the parameters of the flow geometry, a drop may or may not break when colliding with an obstacle in a microdevice. Modeling the flow of one-dimensional trains of monodisperse drops impacting a micro-obstacle, we show numerically that complex dynamics may arise through drop-to-drop hydrodynamic interactions: we observe sequences of breakup events in which the size of the daughter drops created upon breaking mother ones becomes a periodic function of time. We demonstrate the existence of numerous bifurcations between periodic breakup regimes and we establish diagrams mapping the possible breakup dynamics as a function of the governing (physicochemical, hydrodynamic, and geometric) parameters. Microfluidic experiments validate our model as they concur very well with predictions.

1 Introduction

In contrast to classical bulk emulsification techniques for which large quantities of fluid elements are handled at one time,¹ microfluidic technologies allow one to produce monodisperse droplets one by one by using flow-focusing² or T-junction³ geometries and to perform and combine elementary tasks on each of these drops, e.g. fragmentation, dilution, mixing, or encapsulation.^{4,5} By manipulating drops one at a time, this microfluidic toolbox not only offers possibilities for the control of a drop size and internal composition that are expected to be unparalleled but also tremendously impacts material science by paving the way for a *bottom-up* approach to design new material architectures.^{6,7} Nowadays, the literature documents a wide variety of such novel fluid-based materials, e.g. multi-component double emulsions,⁸ high-order emulsions,⁹ microcapsules,¹⁰ and Janus particles.¹¹ Also, using drops as microfluidic analogs of test tubes, it is possible to scale down standard laboratory processes to a square inch device format and to develop efficient high-throughput applications in chemistry, biochemistry, and biology.^{12–21}

To ensure the robustness of applications using microfluidics, many investigations have aimed to understand the physics behind the elementary tasks on drops mentioned

above. In particular, the fragmentation of drops in microdevices is well-documented.^{22–42} This task is indeed widely employed in various applications in diverse fields which include biology, e.g. the screening of compound libraries.⁴³ One can actively break drops into smaller ones using an electric field³⁵ or an optical approach.³⁶ However, most investigations focus on passive (geometry-mediated) breakup methods in which drops may or may not break when reaching a bifurcating path^{22–34} or a micro-obstacle.^{22,38–42} All these works have shown that drop breakup occurs when the capillary number at play exceeds a critical value; yet, establishing a general theoretical framework that completely describes the breakup dynamics has proven to be a difficult task. In our recent works,^{41,42} studying the breakup dynamics of one-dimensional (1-D) trains of drops against rectangular micro-obstacles, we have shown that the use of such geometries allows one to tackle this challenging problem. When the distance between drops λ is large compared with the length of the obstacle L , we have identified the seven dimensionless (hydrodynamic, physicochemical, and geometrical) quantities controlling the dynamics and we have introduced a theoretical framework that rationalizes experimental findings.⁴¹ Within this limit $\lambda \gg L$ that corresponds to the breakup of isolated drops, our model successfully describes the possible breakup regimes observed experimentally, the transition between these regimes, and the volume of the daughter drops created when breakup occurs. Building on this earlier work within the limit $\lambda \ll L$, we have found in this case that the volumes of the daughter droplets depend solely on the geometric features of the breakup geometry.⁴² This behavior which results from drop-to-drop interactions is in sharp contrast with the situation $\lambda \gg L$ for which these volumes not only depend on the

[†] Electronic Supplementary Information (ESI) available: Three Supplementary Movies illustrating sequences of cooperative breakups and a two-page document containing the captions of the Movies and a figure with its caption. This figure shows sequences of numerical breakup regimes as a function of the slug interdistance with other parameters fixed. See DOI: 10.1039/b000000x/^a IPR, UMR CNRS 6251, Campus Beaulieu, Université Rennes 1, 35042 Rennes, France. Fax: 33 2 23 23 67 17; Tel: 33 2 23 23 30 27

[‡] E-mail: laurent.courbin@univ-rennes1.fr

[§] E-mail: pascal.panizza@univ-rennes1.fr

geometry but also on the hydrodynamics and physicochemistry.⁴¹ When $\lambda \ll L$, our study has shown that the number of daughter drops present in each of the two gaps on the sides of the micro-obstacle is very large.⁴² We have therefore assumed the temporal fluctuations of the pressure drops due to the entrance and exit of a daughter drop in the gaps to be negligible compared with the mean values of the pressure drops. We have used this assumption to establish a phenomenological model based on a “mean-field” approach that predicts well experimental findings and helps to rationalize experiments reported in the early literature on the topic.²²

Here, we investigate the general case $\lambda \sim L$ for which the temporal fluctuations of the pressure drops in both gaps are large and can no longer be neglected. For this flow configuration, we expect object-to-object hydrodynamic interactions to induce time-delayed feedback; such feedbacks are, for instance, known to participate in the regulation of droplet traffic at a junction.^{44–52} More generally, the problem is expected to fall into the class of discrete time-delay systems.⁵³ As illustrated in Movies S1–S3 provided in the ESI[†], the breakup of an object can indeed influence the response of the following ones when $\lambda \sim L$. Specifically, we observe in this movie the emergence of complex breakup dynamics that can exhibit periodicity (see Movie S2 and Movie S3 in the ESI[†]). In what follows, we build on the theoretical framework established in recent investigations on droplet breakup against micro-obstacles^{38,41,42} to model the flow and rationalize our observations. We obtain numerical results that demonstrate the emergence of complexity in drop breakup when $\lambda \sim L$. Especially, we predict the existence of regimes in which the size of the daughter drops created upon breaking mother ones varies periodically with the index of the mother drop in the train. We establish diagrams mapping breakup regimes as a function of the physical parameters at play. Both the existence of these periodic breakup regimes and the main features of the predicted breakup diagrams are validated by a set of microfluidic experiments.

2 Numerical simulations

We consider a 1-D train of periodically-spaced drops flowing at a constant velocity v in a microchannel having a rectangular cross-section of height $h = 45 \mu\text{m}$ and width $w = 130 \mu\text{m}$ (see Fig. 1). The train is directed towards a rectangular obstacle of length $L = 300\text{--}700 \mu\text{m}$ and width $30 \mu\text{m}$. This obstacle is parallel to the walls of the main channel and is off-centered so that the two gaps (1) and (2) on each side of the obstacle have different widths w_1 and $w_2 < w_1$ and same height h (Fig. 1). The drops' length and inter-distance are respectively $L_d = 300\text{--}700 \mu\text{m}$ and $\lambda = 400\text{--}2000 \mu\text{m}$. We next refer to these drops which are larger than w and h as “slugs” which periodically collide with the obstacle at a rate

$\nu = v/\lambda$. Upon impact, the front of a slug is deformed so that two fluid-fluid interfaces may invade the two gaps and propagate in them at different velocities.

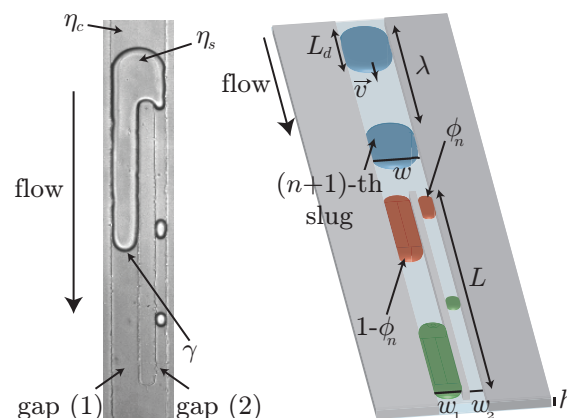


Fig. 1 Top-view photograph of the flow and schematic of the flow geometry defining the geometrical [L, w, h, w_1, w_2], physicochemical [η_c, η_s, γ], and hydrodynamic [L_d, λ, v] parameters of the problem. Also, ϕ_n is the volume fraction of the n -th mother slug flowing in the narrow gap (2).

To model the dynamics of these two-fluid interfaces, we use a theoretical framework that describes both the transport of slugs in microchannels at low Reynolds and capillary numbers and the behavior of isolated slugs impacting micro-obstacles with either circular or rectangular shapes.^{38,41} This framework is based on three flow properties:

(i) v varies as q/S where q is the total flow rate and $S = hw$ is the constant cross-section of the channel,

(ii) Flows of both continuous and slug phases are described by Darcy's laws. Hence, the pressure drop over a portion ℓ of a slug can be written $\Delta p = \frac{\eta_s \ell q}{h^3 w} f(\frac{w}{h})$; η_s is an effective viscosity of the slug⁵⁴ and $f(\frac{w}{h})$ is a dimensionless function that reads $f \approx 12 \left(1 - 0.63 \left(\frac{w}{h}\right)^{-1}\right)^{-1}$ for $h < w$,⁵⁵

(iii) There is a capillary pressure drop $2\frac{\varepsilon\gamma}{w} \left(1 + \frac{w}{h}\right)$ across the curved two-fluid interfaces, i.e. across the front and rear edges of a slug; γ is the surface tension between slug and transporting phases and $\varepsilon = 1$ or -1 depending on whether the front or the rear edge of a slug is considered.

The presence of curved interfaces is taken into account by the capillary pressure. For the sake of simplicity, however, we model the flow considering interfaces that are flat rather than curved. Although strong, such an approximation has allowed us to successfully describe the breakup of isolated slugs.⁴¹

Within this simplified framework, all fluid-fluid interfaces present in one of the gaps (i) of width w_i ($i = 1$ or 2) move at the same velocity $v_i(t)$. The pressure drop across the obsta-

cle then reads $\Delta p(t) = \frac{\eta_c L v_i(t)}{h^2} f\left(\frac{w_i}{h}\right) \left[1 + \left(\frac{\eta_s - \eta_c}{\eta_c}\right) \frac{\ell_i(t)}{L}\right] + \frac{2E_i(t)\gamma}{w_i} \left(1 + \frac{w_i}{h}\right)$, where η_c is the viscosity of the continuous phase. In this expression, at the time t in the gap (i), $\ell_i(t)$ and $E_i(t)$ correspond to the total length occupied by the dispersed phase and the sum of ε over of all two-fluid interfaces, respectively. The origin of time is taken when the front edge of the first slug in a train of slugs collides with the obstacle. The conservation of the total flow rate and the equality of the pressure drop over both gaps allow one to compute $v_i(t)$, thus to predict the positions of all fluid-fluid interfaces in the gap (i) at the time t . In our numerical simulations, time is discretized in δt units of the order of $10^{-3}/\nu$ so that the nature of our findings is not affected by the selected value of δt . We perform our simulations with MATLAB using the flow properties discussed above and the numerical algorithm described below. Whenever an interface enters or exits one of the gaps, $\Delta p(t)$ varies discontinuously which requires to reevaluate $v_i(t)$. Each time $t_n = n/\nu$, the front edge of the n -th slug in the train meets the obstacle and enters the larger gap (1) of width w_1 .[¶] Note that an interface then propagates in the gap (2) only when the pressure drop over the gaps overcomes the capillary pressure required to accommodate the presence of a curved interface in this narrower gap.⁴¹ The rear edge of the n -th slug meets the obstacle a time $t_f = L_d/v$ after t_n . If in the meantime, a two-fluid interface has invaded the narrow gap, has propagated forward and is still present in this gap at the time $t_n + t_f$, the slug breaks into two daughter slugs that flow downstream both gaps. The volume of the daughter slug flowing in the gap (i) of width w_i is then given by:

$$\Omega_i^{(n)} = w_i h \int_{t_n}^{t_n+t_f} v_i(t) dt. \quad (1)$$

When breakup does not occur, the mother slug having a volume $\Omega = L_d w h$ flows in the large gap (1). Consequently, depending on whether breakup occurs or not at $t_n + t_f$, our numerical algorithm places either two new rear edges in both gaps or one rear edge in the large gap. To investigate the influence of drop-to-drop interactions on the fragmentation process, we next study numerically the evolution of the volume fraction $\phi_n = \Omega_2^{(n)}/\Omega$ for trains of colliding slugs as a function of the controlling parameters of the problem. When running a simulation, both gaps are initially empty, i.e. they do not contain any interfaces nor slug phase.

We begin by varying both λ and v , the values of the other parameters [L , w , h , w_1 , w_2 , L_d , η_c , η_s , γ] being constant. As illustrated in Fig. 2, we obtain three main fragmentation regimes. In accordance with our previous work on the breakup of isolated slugs,⁴¹ we observe that fragmentation occurs only for a large enough slug velocity for any λ . Below this critical

speed the slugs do not break (the blue area in Fig. 2 indicates this *no breakup* regime). For large enough slug speeds and high dilutions, i.e. large values of λ , the slugs are sufficiently distant from each other so that the fragmentation of a slug is not influenced by the behavior of the preceding ones; all slugs of a train then break identically. As a result, ϕ_n is constant in this *isolated breakup* regime in which the slugs can be considered as non-interacting hydrodynamically, that is, isolated (the red area in Fig. 2 corresponds to this regime). By contrast, when λ becomes smaller than a critical value that is a function of v , the evolution of ϕ_n with the slug index n exhibits a transient variation for the small values of n , i.e. at early times when the first slugs impact the obstacle and invade the gaps (the green area in Fig. 2 corresponds to this *cooperative breakup* regime). The occurrence of these fluctuations in the response can be qualitatively explained as follows. When the first slug of a train collides with the obstacle, both gaps are solely filled with continuous phase. By contrast, when the next slugs in the train meet the obstacle, one of the two gaps or both of them may contain fluid-fluid interfaces because of the breakup of preceding slugs. The presence of front and rear edges of daughter slugs alters the dynamics of the two-fluid interfaces propagating in these gaps whenever a slug meets the obstacle and thus alters the temporal evolution of the volume of the created daughter slugs. At long times, i.e. large values of n , the response is no longer transient and two behaviors are then observed: ϕ_n is either constant or surprisingly becomes a periodic function of n (see Fig. 2).

We refer to the first case as the *transient cooperative breakup* regime (denoted regime ① in Fig. 2) in which the number and respective positions of the fluid-fluid interfaces present in the two gaps reach steady states. Consequently, all slugs of a train find the same geometric and hydrodynamic configurations when meeting the obstacle. Hence, the slugs all break identically and ϕ_n is constant at long times in the regime ①. The criterion used to distinguish this regime and the *isolated breakup* regime is as follows: the latter regime is obtained when the first slug of a train breaks in the absence of any daughter slugs or interfaces in the gaps and the breakup of all following slugs is identical to that of the first one. In the second case, referred to as *periodic cooperative breakup* regimes, the number and respective positions of the two-fluid interfaces present in the two gaps become periodic functions of n and so does ϕ_n . Figure 2 shows an example (regime ④) of such periodic cooperative regimes; the number used to denote a periodic cooperative regime corresponds to its period $T \geq 2$ which is the number of daughter slugs per cycle.

We next discuss our results using the capillary number $C = \frac{\eta_c v}{\gamma}$ that compares the magnitude of viscous and surface forces and is generally the governing dimensionless quantity in problems dealing with the breakup of drops or bubbles.⁵⁶

To thoroughly study the problem, we run numerical simula-

[¶] This situation requires that experiments are performed at constant flow rates.

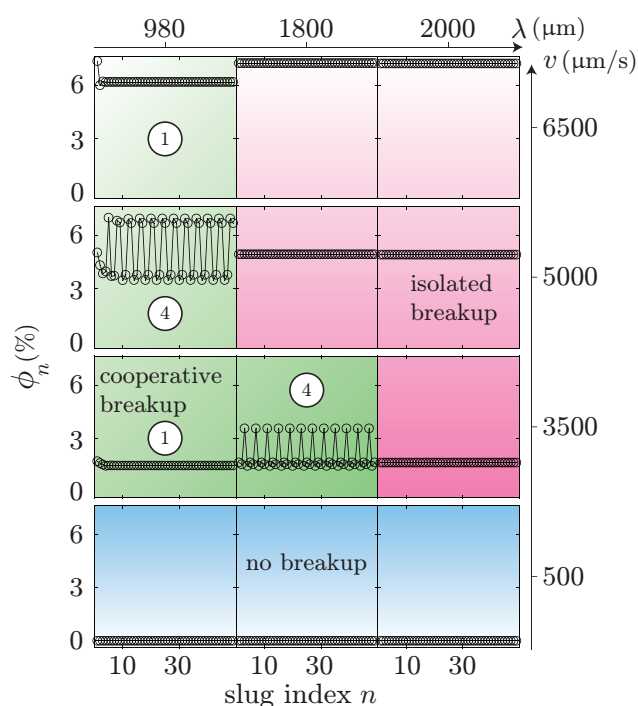


Fig. 2 Numerical variations of ϕ_n for a sequence of daughter slugs produced upon breakup in the narrow gap as a function of the index of the mother slug n for twelve sets of parameters (λ, v) as indicated in the figure. The shaded colors denote the three observed behaviors: (blue) no breakup, (red) isolated breakup, and (green) cooperative breakup. The regimes ① and ④ denote transient and periodic cooperative regimes, respectively. The simulations are conducted with $L_d = 280 \mu\text{m}$, $w_1 = 70 \mu\text{m}$, $w_2 = 30 \mu\text{m}$, $L = 700 \mu\text{m}$, $\eta_c = 3 \text{ mPa s}$, $\eta_s = 12 \text{ mPa s}$, and $\gamma = 6.5 \text{ mN m}^{-1}$.

tions for different values of L and L_d and we report the results in diagrams mapping the response in the plane $(\frac{\lambda}{L}, C)$. These diagrams reported in Fig. 3 and Fig. 4 share similar features which indicate the generality of the reported phenomena:

(i) For any combination of obstacle length and slug size, breakup occurs only when the capillary number exceeds a critical value. Below this value, the *no breakup* regime is solely observed,

(ii) When breakup occurs, the observation of *cooperative breakup* regimes requires λ/L to be small enough to introduce slug-to-slug hydrodynamic interactions. For large values of λ/L , only *isolated breakup* regimes are obtained,

(iii) Both *transient* (regime ①) and *periodic* (period $T \geq 2$) *cooperative breakup* regimes are obtained for large enough capillary number and small enough ratio λ/L .

Our results show that the period of the periodic cooperative regimes is a function of the governing parameters that can be larger than 4; the period can be as large as eight daughter

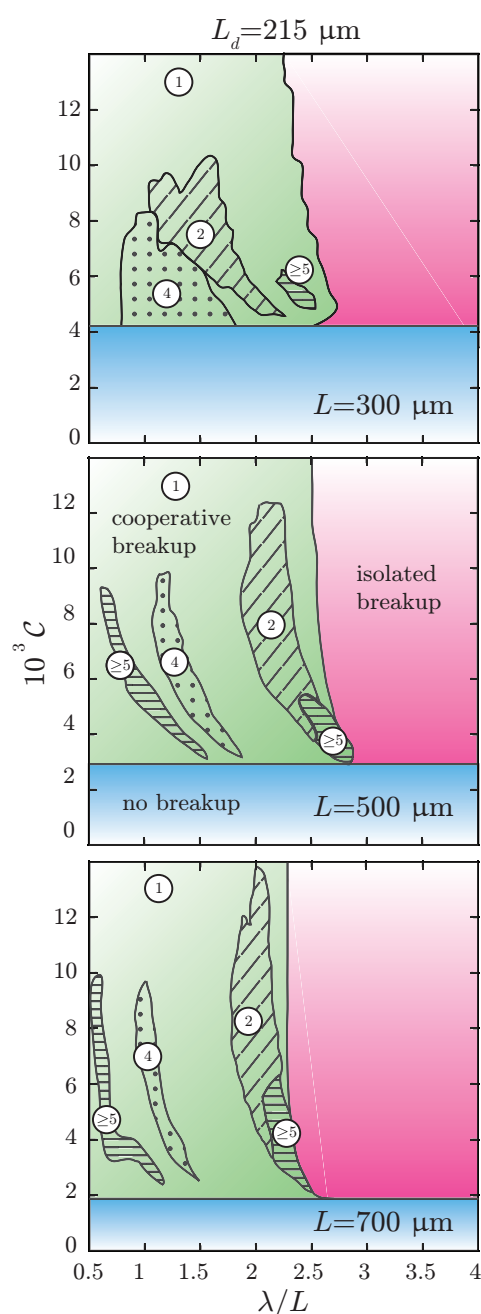


Fig. 3 Numerical diagrams mapping the different hydrodynamic regimes in the plane $(\frac{\lambda}{L}, C)$ for $L_d = 215 \mu\text{m}$ and increasing values of L from the top to the bottom panel as indicated in the figure. The other parameters are identical to those of Fig. 2. Like in Fig. 2, the shaded colors indicate the three main breakup regimes: (blue) no breakup, (red) isolated breakup, and (green) cooperative breakup. The regime ① corresponds to the transient cooperative breakup regime. Each of the patterns denotes the period $T \geq 2$ of a periodic cooperative regime: Oblique dashed lines ($T = 2$), dots ($T = 4$), and horizontal lines $T \geq 5$. T also corresponds to the number used to denote a periodic regime as shown in the figure.

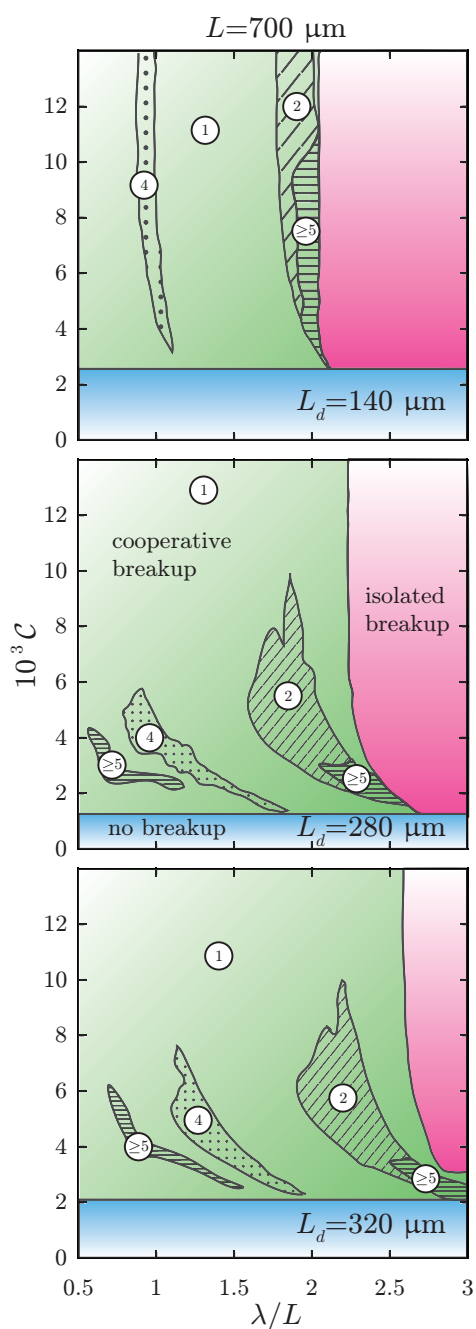


Fig. 4 Numerical diagrams mapping the different hydrodynamic regimes in the plane $(\frac{\lambda}{L}, C)$ for $L = 700 \mu\text{m}$ and increasing values of L_d from the top to the bottom panel as indicated in the figure. The colors, patterns and other parameters are identical to those of Fig. 2 and Fig. 3.

slugs per cycle (data shown in Fig. S1 of the ESI[†]) which indicates the existence of long range correlations between successive breakup events. The domain of existence of cooperative breakup regimes is also significantly influenced by the obstacle length and slug size. For a value of λ/L and L_d , figure 3 shows that a periodic cooperative regime spans a wider range of C as L increases. By contrast, as shown in Fig. 4, when L is fixed, increasing L_d for a value of λ/L tends to reduce the domains of existence of these regimes when C is changed.

3 Experiments

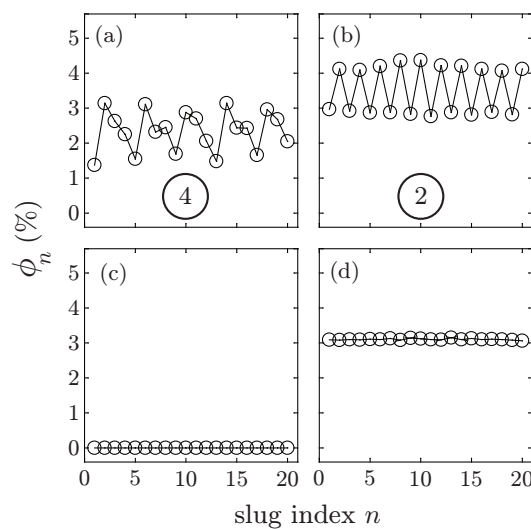


Fig. 5 Experimental variations of the volume fraction ϕ_n as a function of the index of the mother slug n for four sets of parameters $[\lambda, v, L_d]$: (a) cooperative breakup regime ④ [$\lambda = 702 \pm 39 \mu\text{m}$, $v = 10275 \pm 173 \mu\text{m s}^{-1}$, $L_d = 286 \pm 11 \mu\text{m}$], (b) cooperative breakup regime ② [$\lambda = 1246 \pm 43 \mu\text{m}$, $v = 11653 \pm 289 \mu\text{m s}^{-1}$, $L_d = 262 \pm 16 \mu\text{m}$], (c) no breakup [$\lambda = 448 \pm 19 \mu\text{m}$, $v = 6377 \pm 260 \mu\text{m s}^{-1}$, $L_d = 281 \pm 13 \mu\text{m}$], (d) isolated breakup [$\lambda = 654 \pm 35 \mu\text{m}$, $v = 11312 \pm 382 \mu\text{m s}^{-1}$, $L_d = 254 \pm 13 \mu\text{m}$].

To validate our model and the resulting numerical predictions, we carry out microfluidic experiments with planar devices made of poly-dimethylsiloxane (PDMS-Sylgard 184 purchased from Dow Corning) using soft lithography techniques.⁵⁷ As briefly described below, the features of our experimental set-up are similar to the geometry used for the numerical simulations (see Fig. 1). A flow focusing geometry² is employed to generate a train of periodically-spaced monodisperse slugs flowing in a channel having a rectangular cross-section (height $h = 45 \mu\text{m}$ and width $w = 130 \mu\text{m}$). The 1-D train of slugs is then directed towards a rectangular obstacle of length $L = 700 \mu\text{m}$, parallel to the walls of the channel. The obstacle is off-centered and the two gaps on its sides are

$w_1 = 70 \mu\text{m}$ and $w_2 = 30 \mu\text{m}$. The fluid-fluid system is deionized water (Millipore, $18 \text{ M}\Omega \text{ cm}$) dispersed in hexadecane (Sigma-Aldrich) that serves as transporting phase. The water phase contains 15 g/L of a surfactant (Sodium Dodecyl Sulfate, Sigma). The two fluids are injected at controlled flow rates using independently adjusted syringe pumps (PHD 2000, Harvard Apparatus). For this two-fluid system, the viscosities and the surface tension between phases are $\eta_c = 3 \text{ mPa s}$, $\eta_s = 12 \text{ mPa s}$, and $\gamma = 6.5 \text{ mN m}^{-1}$.⁴¹ An additional injection (or withdrawal) of continuous phase is conducted in a dilution module placed far upstream from the obstacle so that the flow is steady near the obstacle. This module enables to control the distance λ between slugs, thus their speed v , while maintaining their size L_d and production rate ν unchanged.⁵⁸ Images of the flow are recorded in the vicinity of the obstacle with a high-speed camera (Phantom V7) working at 1000 frames/s. The values of the parameters L_d , v , λ and the volume fraction ϕ_n are obtained from image analysis using a custom-written MATLAB software. In all our experiments, the Reynolds and capillary numbers are small and span the ranges $10^{-2} - 10^{-1}$ and $10^{-4} - 10^{-2}$, respectively.

Quantitative measurements of the volume fraction ϕ_n confirm the experimental existence of cooperative breakup regimes illustrated qualitatively in Movies S1–S3 in the ESI[†] and predicted numerically (see Fig. 5(a) and (b) showing two examples of experimental periodic breakups). Also, figure 5(c) shows that the slugs do not break when their speed does not exceed a critical value as found numerically. For speeds larger than the critical one, isolated breakup is observed when λ is large enough to prevent slug-to-slug interactions [Fig. 5(d)]. Movies corresponding to no-breakup and isolated breakup regimes can be found as Supplementary Material of one of our recent work⁴¹. Hence, the main features of our numerical predictions discussed in section 2 are observed experimentally.

To further validate our numerical model, we proceed as follows. When a steady train of slugs having the desired slug size is obtained, we vary the additional flow rate in the dilute module while maintaining all other flow rates unchanged. This method for which L_d and ν are set while $v = \lambda\nu$ is adjusted, allows us to investigate the problem experimentally along straight dilution lines and to establish diagrams mapping the response in the plane $(\frac{\lambda}{L}, \mathcal{C})$. The criterion used to distinguish transient cooperative breakups and isolated breakups is identical to the one defined in section 2 for our numerical simulations. In Fig. 6, we report our experimental results along with numerical data in a diagram plotted in the plane $(\frac{\lambda}{L}, \mathcal{C})$ with identical values of governing parameters. Each set of measurements is performed along a given dilution line and is represented by a given symbol. The colors and patterns used for these symbols are identical to those used for our numerical diagrams. These colors and patterns allow one to identify the

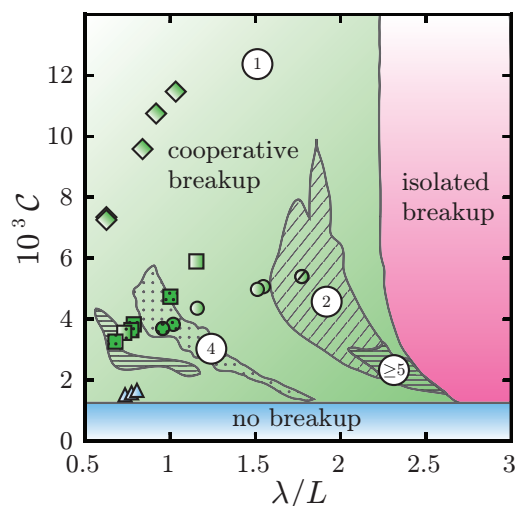


Fig. 6 Comparison between the numerical diagram mapping the three hydrodynamic regimes in the plane $(\frac{\lambda}{L}, \mathcal{C})$ for $L_d = 280 \mu\text{m}$ and $L = 700 \mu\text{m}$ (middle plot in Fig. 4) and four sets of measurements conducted with the same value of L and an average slug size $280 \mu\text{m}$ with a standard deviation $\sigma = 13 \mu\text{m}$. The colors, patterns and other parameters are identical to those of Figs. 4. Each set of measurements is performed along a dilution line and is represented by a symbol (diamonds, squares, circles and triangles).

nature of the three main observed regimes [no breakup (blue), isolated breakup (red), and cooperative breakup (green)] and the period T of the possible periodic regimes. As indicated in Fig. 6, the oblique dashed, dotted, and horizontal solid lines stand for regimes with $T=2$, $T=4$, and $T \geq 5$, respectively. As shown in this figure, despite the strong approximations in our simple physical model, the predictions obtained for the domains of existence of the different breakup regimes concur well with experiments conducted for the same obstacle length and slug size. Also, figure 6 shows that the numerical predictions of the periods T of periodic cooperative regimes compare well with experimental data. Unfortunately, we could not manage to report experimental observations of periodic regimes with periods larger than 4 as their occurrence is predicted numerically in very narrow regions of the dilution lines.

4 Conclusions

To conclude, we have shown that the breakup dynamics of a 1-D train of drops against a micro-obstacle can be complex. Especially, numerical simulations and experimental observations show the emergence of cooperative effects between drops: we report regimes in which the volume of the daughter droplets created upon breaking mother ones becomes a time-periodic function. As seen in investigations of droplet traffic in mi-

crofluidic networks,^{47–50} the occurrence of periodic regimes separated by bifurcations results from the iteration of simple rules and the existence of hydrodynamic feedback between drops. Inherent in microfluidics, such time-delayed feedbacks originate from the alteration of the hydrodynamic resistance of a channel by the presence of drops flowing in it. Hence, the breakup of a drop may be influenced by the behavior of the preceding ones in a train of drops. From the standpoint of nonlinear physics, cooperative breakups allow one to investigate time-delay effects on a continuous variable (here ϕ_n) in a temporally discrete system. These findings could also help the design of commercial obstacle-mediated breakup devices as they offer possibilities for tailoring emulsions and foams having a multimodal distribution of sizes.^{59,60}

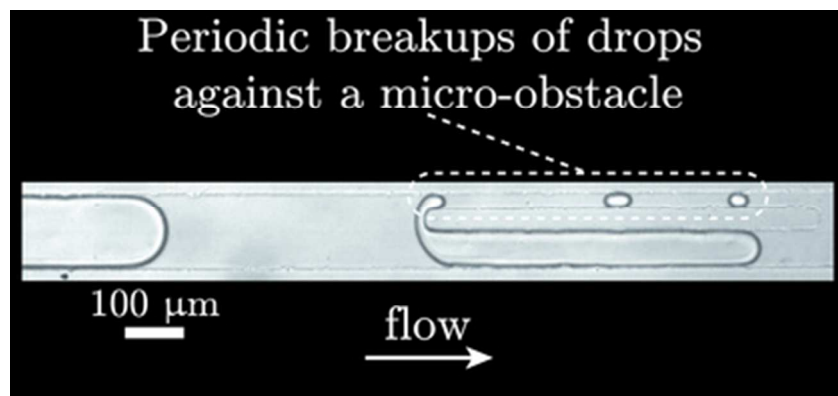
Acknowledgements

This work was initiated following a discussion one of us (P.P.) had with L. Baraban and N. Bremond a few years ago. We thank A. Saint-Jalmes for his kind help with viscosity and surface tension measurements.

References

- 1 F. Leal-Calderon, V. Schmitt and J. Bibette, *Emulsion Science-Basic: Principles*, Springer, New York, 2007.
- 2 S. L. Anna, N. Bontoux and H. A. Stone, *Appl. Phys. Lett.*, 2003, **82**, 364.
- 3 P. Garstecki, M. B. Fuerstman, H. A. Stone and G. M. Whitesides, *Lab Chip*, 2006, **6**, 437.
- 4 M. Joanicot and A. Ajdari, *Science*, 2005, **309**, 887.
- 5 R. Seemann, T. Brinkmann, T. Pfohl and S. Herminghaus, *Rep. Prog. Phys.*, 2012, **75**, 016601.
- 6 R. K. Shah, H. C. Shum, A. C. Rowat, D. Lee, J. J. Agresti, A. S. Utada, L.-Y. Chu, J.-W. Kim, A. Fernández-Nieves, C. J. Martínez and D. A. Weitz, *Materials Today*, 2008, **11**, 18.
- 7 W. Engl, R. Backov and P. Panizza, *Curr. Opin. Colloid Interface Sci.*, 2008, **13**, 206.
- 8 S. Okushima, T. Nisisako, T. Torii and T. Higushi, *Langmuir*, 2004, **20**, 9905.
- 9 L. Y. Chu, A. S. Utada, R. K. Shah, J.-W. Kim and D. A. Weitz, *Angew. Chem. Int. Ed.*, 2007, **46**, 8970.
- 10 A. S. Utada, E. Lorenceau, D. R. Link, P. D. Kaplan, H. A. Stone and D. A. Weitz, *Science*, 2005, **308**, 537.
- 11 C.-H. Chen, R. K. Shah, A. R. Abate and D. A. Weitz, *Langmuir*, 2009, **25**, 4320.
- 12 Y. H. Chang, G. B. Lee, F. C. Huang, Y. Y. Chen and J. L. Lin, *Biomed Microdevices*, 2006, **8**, 215.
- 13 S. Haeberle and R. Zengerle, *Lab Chip*, 2007, **7**, 1094.
- 14 R. B. Fair, *Microfluid. Nanofluid.*, 2007, **3**, 245.
- 15 S.-Y. Teh, R. Lin, L.-H. Hung and A. P. Lee, *Lab Chip*, 2008, **8**, 198.
- 16 I. Barbulovic-Nad, H. Yang, P. S. Park and A. R. Wheeler, *Lab Chip*, 2008, **8**, 519.
- 17 E. M. Miller and A. R. Wheeler, *Anal. and Bioanal. Chem.*, 2009, **393**, 419.
- 18 J. J. Agresti, E. Antipov, A. R. Abate, K. Ahn, A. C. Rowat, J. C. Baret, M. Marquez, A. R. Klibanov, A. D. Griffiths and D. A. Weitz, *Proc. Nat. Acad. Soc.*, 2010, **107**, 4004.
- 19 N. Lorber, F. Sarrazin, P. Guillot, P. Panizza, A. Colin, B. Pavageau, C. Hany, P. Maestro, S. Marre, T. Delclos, C. Aymonier, P. Subra, L. Prat, C. Gourdon and E. Mignard, *Lab Chip*, 2011, **11**, 779.
- 20 L. Baraban, F. Bertholle, M. L. Salverda, N. Bremond, P. Panizza, J. Baudry, J. A. de Visser and J. Bibette, *Lab Chip*, 2011, **11**, 4057.
- 21 M. T. Guo, A. Rotem, J. A. Heyman and D. A. Weitz, *Lab Chip*, 2012, **12**, 2146.
- 22 D. R. Link, S. L. Anna, D. A. Weitz and H. A. Stone, *Phys. Rev. Lett.*, 2004, **92**, 054503.
- 23 M. De Menech, *Phys. Rev. E:Stat., Nonlinear, Soft Matter Phys.*, 2006, **73**, 031505.
- 24 L. Ménétrier-Deremble and P. Tabeling, *Phys. Rev. E:Stat., Nonlinear, Soft Matter Phys.*, 2006, **74**, 035303R.
- 25 M. Yamada, S. Doi, H. Maenaka, M. Yasuda and M. Seki, *J. Colloid Interface Sci.*, 2008, **321**, 401.
- 26 A. M. Leshansky and L. M. Pismen, *Phys. Fluids*, 2009, **21**, 023303.
- 27 M.-C. Jullien, M.-J. Tsang Mui Ching, C. Cohen, L. Ménétrier and P. Tabeling, *Phys. Fluids*, 2009, **21**, 072001.
- 28 T. Fu, Y. Ma, D. Funfschilling and H. Z. Li, *Chem. Eng. Sci.*, 2011, **66**, 4184.
- 29 A. Bedram and A. Moosavi, *Eur. Phys. J. E*, 2011, **34**, 78.
- 30 Y. Wu, T. Fu, C. Zhu, Y. Lu, Y. Ma and H. Z. Li, *Microfluid. Nanofluid.*, 2012, **13**, 723.
- 31 A. M. Leshansky, S. Afkhami, M.-C. Jullien and P. Tabeling, *Phys. Rev. Lett.*, 2012, **108**, 264502.
- 32 M. Samie, A. Salari and M. B. Shafii, *Phys. Rev. E:Stat., Nonlinear, Soft Matter Phys.*, 2013, **87**, 053003.
- 33 X. Wang, C. Zhu, T. Fu and Y. Ma, *Chem. Eng. Sci.*, 2014, **111**, 244.
- 34 T. Fu, Y. Ma and H. Z. Li, *AIChE*, 2014, **60**, 1920.
- 35 D. R. Link, E. Grasland-Mongrain, A. Duri, F. Sarrazin, Z. Cheng, G. Cristobal, M. Márquez and D. A. Weitz, *Angew. Chem. Int. Ed.*, 2006, **45**, 2556.
- 36 C. N. Baroud, M. Robert de Saint Vincent and J.-P. Delville, *Lab Chip*, 2007, **7**, 1029.
- 37 T. Cubaud, *Phys. Rev. E:Stat, Nonlinear, Soft Matter Phys.*, 2009, **80**, 026307.
- 38 S. Protière, M. Z. Bazant, D. A. Weitz and H. A. Stone, *EPL*, 2010, **92**, 54002.
- 39 C. Chung, K. H. Ahn and S. J. Lee, *J.Non-Newtonian Fluid Mech.*, 2009, **162**, 38.
- 40 C. Chung, M. Lee, K. Char, K. H. Ahn and S. J. Lee, *Microfluid. Nanofluid.*, 2010, **9**, 1151.
- 41 L. Salkin, L. Courbin and P. Panizza, *Phys. Rev. E: Stat., Nonlinear, Soft Matter Phys.*, 2012, **86**, 036317.
- 42 L. Salkin, A. Schmit, L. Courbin and P. Panizza, *Lab Chip*, 2013, **13**, 3022.
- 43 J. Clausell-Tormos, A. D. Griffiths and C. A. Merten, *Lab Chip*, 2010, **10**, 1302.
- 44 F. Jousse, R. Farr, D. R. Link, M. J. Fuerstman and P. Garstecki, *Phys. Rev. E:Stat., Nonlinear, Soft Matter Phys.*, 2006, **74**, 036311.
- 45 M. Schindler and A. Ajdari, *Phys. Rev. Lett.*, 2008, **100**, 044501.
- 46 M. Belloul, W. Engl, A. Colin, P. Panizza and A. Ajdari, *Phys Rev. Lett.*, 2009, **102**, 194502.
- 47 T. Glawdel, C. Elbuken and C. L. Ren, *Lab Chip*, 2011, **11**, 3774.
- 48 D. A. Sessoms, A. Amon, L. Courbin and P. Panizza, *Phys. Rev. Lett.*, 2010, **105**, 154501.
- 49 O. Cybulski and P. Garstecki, *Lab Chip*, 2010, **10**, 484.
- 50 N. Champagne, R. Vasseur, A. Montourcy and D. Bartolo, *Phys. Rev. Lett.*, 2010, **105**, 044502.
- 51 P. Parthiban and S. A. Khan, *Biomicrofluidics*, 2013, **7**, 044123.
- 52 J. Maddala, S. A. Vanapalli and R. Rengaswamy, *Phys. Rev. E*.
- 53 T. Erneux, *Applied Delay Differential Equation*, Springer, New York,

-
- 2009.
- 54 The effective viscosity is a free parameter that accounts for additional viscous dissipation in the thin films of continuous phase around the slug, in the corners of the rectangular geometry and inside the slug⁴¹.
- 55 H. Bruus, *Theoretical Microfluidics*, Oxford University Press, Oxford, 2008.
- 56 H. A. Stone, *Annu. Rev. Fluid Mech.*, 1994, **26**, 65.
- 57 J. C. McDonald, D. C. Duffy, J. R. Anderson, D. T. Chiu, H. Wu, O. J. A. Schueller and G. M. Whitesides, *Electrophoresis*, 2000, **21**, 27.
- 58 D. A. Sessoms, M. Belloul, W. Engl, M. Roche, L. Courbin and P. Panizza, *Phys. Rev. E:Stat., Nonlinear, Soft Matter Phys.*, 2009, **80**, 016317.
- 59 M. Seo, Z. Nie, S. Xu, P. C. Lewis and E. Kumacheva, *Langmuir*, 2005, **21**, 4773.
- 60 M. Hashimoto, P. Garstecki and G. M. Whitesides, *Small*, 2007, **3**, 1792.



We present a model describing the complex breakup dynamics of one-dimensional trains of drops against rectangular micro-obstacles.
35x16mm (300 x 300 DPI)